Supplement of Biogeosciences, 16, 663–680, 2019
https://doi.org/10.5194/bg-16-663-2019-supplement

Biogeosciences Open Access EGU

Supplement of

Modeling anaerobic soil organic carbon decomposition in Arctic polygon tundra: insights into soil geochemical influences on carbon mineralization

Jianqiu Zheng et al.

Correspondence to: David E. Graham (grahamde@ornl.gov)

Data synthesis

Site description and soil incubations

The Barrow Environmental Observatory (BEO) in Utqiaġvik **(**Barrow) Alaska, USA consists of thaw lakes, drained thaw lake basins and interstitial tundra with a polygonal landscape of microtopographic features created by ice wedges. As part of the Next Generation Ecosystem Experiments Arctic project (http://ngee-arctic.ornl.gov/), frozen soil cores were collected from different microtopographic positions of Low-centered, Flat-centered, and High-centered polygons (LCP, FCP, HCP) in the wet tundra. LCPs are characterized by narrow, saturated troughs, raised rims, and wet, sometimes saturated centers (Figure 1) (French, 2007; Liljedahl et al., 2016). We previously performed short-term incubations of LCP soils under anoxic, environmentally relevant conditions to measure rates and temperature sensitivities of CO_2 and CH_4 production (Roy Chowdhury et al., 2015). FCPs represent transitional polygons with melting ice wedges, minimal rims, moderately dry centers, and disconnected troughs. Incubations of FCP soils demonstrated both methanogenesis and methane oxidation potential, with high levels of activity at the transition zone (Zheng et al., 2018). Finally, HCPs have well drained centers and low, saturated troughs. Incubations of HCP soils showed significant fermentation, methanogenesis and anaerobic respiration in the saturated troughs (Yang et al., 2016), contrasted with aerobic respiration and minimal methanogenesis in the centers (Roy Chowdhury et al, in preparation). These controlled incubations provided critical information on anaerobic SOM decomposition processes across a gradient of soil with fine-scale variability in thermal and hydrological regimes.

Incubation datasets from 8 soil cores, divided in 126 soil microcosms associated with 14 treatments (soil microtopographic features × soil layer) were included in this synthesis to represent the microtopographic heterogeneity of polygonal tundra. Soil cores were previously sectioned into organic, mineral, cryoturbated transition zone (if identified) and permafrost for microcosm incubations. The period of anoxic incubation in these studies ranged from 45 to 90 days with an average of approximately 60 days at field-relevant temperatures of -2, +4 and +8 °C. Cumulative CO_2 and CH_4 production data were collected at different time intervals during incubations. More details on the microcosm construction, headspace CO_2 and CH_4 sampling, and rate calculations can be found in the corresponding publications (Roy Chowdhury et al., 2015; Herndon et al., 2015) and datasets (Zheng and Graham, 2018; Zheng et al., 2017). Changes in exchangeable Fe(II), water extractable organic carbon (WEOC), low molecular weight organic acids, and pH of soil microcosms during anoxic incubation were summarized previously in publications (Herndon et al., 2015) and datasets (Zheng and Graham, 2018; Herndon et al., 2017).

Data processing and statistics

In order to compare the cumulative carbon loss (as both CO_2 and CH_4) from different polygonal and microtopographic features and different soil layers, measurements from triplicate microcosms were pooled together and fitted with hyperbolic, sigmoidal, exponential or linear functions that best describe the dynamic. The cumulative CO_2 and CH_4 production within 60 days of anaerobic incubation was directly calculated from each fitted curve and used for descriptive statistical analyses.

Individual curve fitting for each microcosm was used to best represent the rate changes of CO_2 and CH_4 production. CO_2 production followed hyperbolic curves with immediate CO_2 release for all LCP, FCP and HCP trough samples. CO_2 production from HCP center samples experienced time lags for approximately 10 days for the mineral layer, and 45 days for the permafrost. CH_4 production was also associated with varying time lags before reaching maximum rates, and the lag is most profound in HCP samples, between 6 to 20 days. The rate of gas production estimated from hyperbolic curve fitting predicts a continuously decreasing rate, while sigmoidal curve fitting with an initial delay predicts a maximum rate after the lag time. Here, we used the derivatives of nonlinear curve fitting to calculate initial rates of gas production. For hyperbolic fittings, the maximum rate is calculated at day 0. For sigmoidal fittings, the maximum rate is calculated by setting the third derivative to zero. The temperature dependence was calculated using conventional Q_{10} by taking the ratio of maximum production rates at 8 and -2 °C based on triplicate measurements. There was no significant difference between Q_{10} values estimated by this simple difference method versus regression using rates at -2, +4 and +8 °C. Data fitting and statistical analyses were conducted and validated using R 3.4.0 (The R Foundation for Statistical Computing) and Python 3.6.0 (Python Software Foundation) computing environments. A complete list of packages and libraries used here can be found in the following references (Venables and B.D., 2002; Hunter, 2007; Oliphant, 2007; Sarkar, 2008; van der Walt et al., 2011; Wickham, 2009; Wickham et al., 2017).

Synthesized soil geochemical characteristics

Soil samples used in this study represent a wide range of SOC content, from 2% to 39%, with the highest SOC found in surface organic layers. In correlation analysis of initial soil geochemical characteristics, both WEOC and TOAC showed strong correlation with SOC content among

examined soil cores and across soil depth (Table S4). Decomposition generated limited changes in WEOC. WEOC represents 0.26% to 2.6% of total SOC among all test soils, and this ratio remained constant before and after anoxic incubations (Figure S3a). Higher incubation temperatures showed minimal effect on the WEOC/SOC quotient, and a temperature response trend remained insignificant. On the other hand, TOAC showed much more dynamic changes among different soils and different incubation temperatures. TOAC increased by 5% to 175% in organic soils, and 2% to 60% in the transition zone and permafrost from LCP and HCP centers (Figure S3b). In most mineral soils, TOAC drastically decreased by up to 90%, partially contributing to the depletion of WEOC after the anoxic incubations. These results indicate that WEOC was usually in a steady state, while TOAC varied substantially due to microbial activity.

Good correlations between soil organic carbon (SOC, WEOC and TOAC) and soil moisture were found, indicating the importance of soil moisture in controlling carbon substrate availability (Table S2). High organic carbon content and high soil moisture are associated with organic and permafrost soil, while mineral soils are much drier with lower organic carbon content. Fe(II) concentration is measured as a proxy of soil redox potential, and it is most closely related to soil pH (Table S4).

Temperature response of CO_2 and CH_4 production

Cumulative production of both CO_2 and CH_4 showed close correlation with soil carbon content (represented as SOC, WEOC and TOAC) on a dry soil mass basis, as well as soil moisture (Table S4). The maximum values of cumulative CO_2 production were 756 and 534 μmol g^{-1} C at 8 and -2°C, exceeding the median values at corresponding temperature by 5 and 8 times, respectively. The maximum cumulative CH_4 production was 198 μmol g^{-1} C from the organic layer of LCP center at 8 °C, approximately 123 times the median value among the rest of the samples. Cumulative CH_4 production from the same soil was 9.2 μmol g^{-1} C when incubated at -2 °C, 9 times the median rate among the remaining samples.

Initial production rates of CO_2 and CH_4 varied significantly across organic, mineral and permafrost soil layers ($p<0.001$ and $p<0.001$, respectively). Temperature showed a substantial positive effect on CO_2 and CH_4 production rates ($p=0.02$ and $p=0.04$, respectively). A significant temperature × soil layer interaction effect was found on CO_2 production rate, but not on CH_4 production rate (Table S5), suggesting CH_4 production might be more sensitive to constraints from additional environmental conditions.

A Q_{10} value was calculated for each condition to further assess the temperature dependency of CO_2

and CH_4 production (Figure S4). The calculated Q_{10} values of CO_2 production from organic soil were within a narrow range between 4.6 and 5.0. Mineral soils with lower SOC content showed a wider range of Q_{10} values (from 3.6 to 7.3). Permafrost showed significantly lower Q_{10} than both organic and mineral layers (Table S6). Methanogenesis had much larger variations in estimated Q_{10} values. Organic soils had a Q_{10} value between 18.5 and 48.1, while in mineral soils and permafrost, the average Q_{10} values were 7.1 and 1.6, respectively. Using Q_{10} values to simulate the temperature dependence of processes might work for CO_2 production, but could generate significant errors in predicting CH_4 production.

Model structure

Representation of carbon pool cascade

The CLM-CN decomposing pool cascade (Converging Trophic Cascade) was adopted to represent upstream carbon flow entering the DOC pool (Thornton and Rosenbloom, 2005). Characterizations of SOC during short-term incubations provided insufficient information to partition SOC into chemically distinct pools. Thus, we took the empirical approach in representing bulk SOC during anaerobic decomposition with a simplified carbon cascade including 4 SOM pools (Figure 1). This approach uses discrete SOM pools with modified first-order-decay, and the change in carbon pools is as follow (Koven et al., 2013):

$$\frac{\partial C_i}{\partial t} = \sum_{j \neq i} (1 - r_j) T_{ji} K_j C_j - k_i C_i$$

where C_i is the amount of carbon in pool i (mmol C kg^{-1} H_2O), k_i is the decay constant for pool i (s^{-1}); T_{ji} is the fraction of carbon from pool j entering pool i with a respiration fraction r_j lost as respiration. Under anoxic conditions, the respiration fraction r_j is further split into a direct and an indirect fraction. The direct fraction directly respires to CO_2, while the indirect fraction produces labile carbon entering DOC pool that would further respire as CO_2 or CH_4 via methanogenesis and iron reduction. Here we assume 80% of the original respired fraction enters DOC pool, while the remaining 20% respired as CO_2 (Tang et al., 2016). CO_2 production is required in anaerobic systems for microbial biomass formation: forming reduced cellular components such as lipids must be offset by CO_2 production to balance electrons in the system. Thus, the revised carbon decomposition cascade structure and parameters can be summarized as follow:

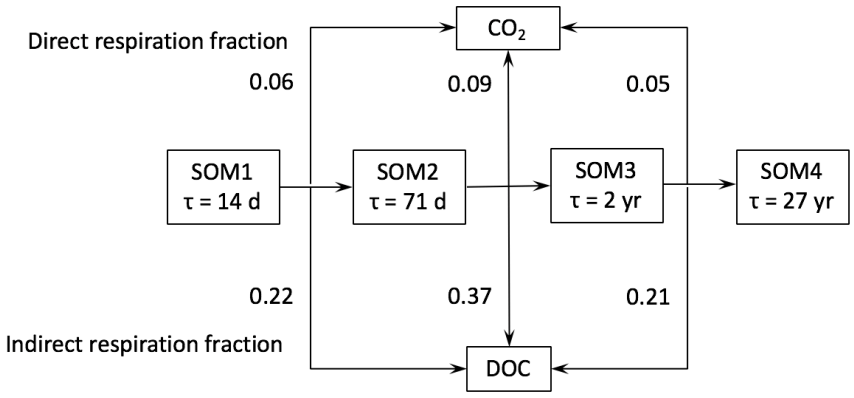

The available carbon (DOC) is further fermented into acetate, CO_2 and H_2 as a lumped fermentation process (Appendix A, reaction A1). The fermentation reaction also follows first-order-decay kinetics with fixed stoichiometry, in which 1/3 of the fermented carbon is converted to CO_2. A single molecular formula (acetate) is used here to represent fermentation-produced organic acids.

Representation of methanogenesis and iron reduction

Fermentation products (acetate and H_2) are further decomposed via methanogenesis and iron reduction. We use a thermodynamically-based approach to parameterize the reaction kinetics. The microbial growth equations of methanogens and iron reducers are formed by combining electron donor (oxidation) half reactions, electron acceptor (reduction) half reactions, and cell synthesis reactions following bioenergetics (Jin and Bethke, 2007). We assume that the molecular formula for biomass is constant among all microbial functional groups as $C_5H_7O_2N$, thus biomass growth is built into the reaction stoichiometry (Appendix A, reaction A2 and A3) and the rate of methanogenesis can be calculated as:

$$\frac{\partial x}{\partial t} = k_{max} x \frac{m_D}{k_D + m_D} f(G)$$

where k_{max} is the kinetic rate constant (s^{-1}), x is concentration of biomass (mmol biomass kg^{-1} H_2O), m_D and k_D are the concentration and half saturation constant of electron donors. $f(G)$ is a thermodynamic factor that goes to zero when the reaction is thermodynamically unfavorable. The microbial biomass synthesized during redox reactions can be expressed as

$$\frac{dx}{dt} = (\mu - D)x$$

where x is biomass concentration (mmol biomass kg^{-1} H_2O), μ is the specific growth rate (s^{-1}), and D is the biomass decay rate (s^{-1}).

Iron reduction (Appendix A, reaction A4 and A5) results in dissolution of amorphous ferric hydroxides $Fe(OH)_{3(s)}$ (Appendix A, reaction A6), thus a modified rate expression is required (Jin and Kirk, 2016):

$$\frac{\partial x}{\partial t} = k_{max} x \frac{k_{surf}}{k_{surf} + x/m_{surf,avail}} \frac{m_D}{k_D + m_D} f(G)$$

where $m_{surf,\ avail}$ is the concentration of microbially-available surface sites on amorphous $Fe(OH)_{3(s)}$ (mmol kg^{-1} H_2O), k_{surf} is a constant represents the interaction of biomass with available surface sites on $Fe(OH)_{3(s)}$ (mol biomass mol^{-1} bioavailable surface sites).

Representation of pH buffering with WHAM humic ion-binding model

To mediate proton transfer during redox reactions, we introduced a proton-binding component into the model for chemical equilibrium calculations. Briefly, the average proton-binding characteristics of mixed SOM were parameterized using the Windermere Humic Aqueous Model (WHAM, Tipping, 1994; Tipping, 1998). WHAM parametrization was based on a discrete distribution of binding sites, with four sites representing carboxylic groups and four sites reprinting phenolic groups on organic compounds. A total of 8 representative equilibrium constants were included in the model, as both monoprotic and biprotic weak acids. We use WHAM parametrization to simulate proton-binding by SOM, with the following two assumptions for model simplicity: first, the number of proton-binding sites of each weak acid is linearly correlated with organic carbon content of the acid. Second, all monoprotic and biprotic weak acids are at the same concentration to represent a complex mixture of SOM. Based on the above two assumptions, the total buffering capacity [β, mol L^{-1} (H^+ or OH^-) pH^{-1}] containing i monoprotic and n biprotic weak acids can be calculated as:

$$\beta = 2.303\,[H^+]\,(1 + \sum C_i \left(\frac{K_a}{(K_a + [H^+])^2}\right)_i + \sum C_n \left(\frac{K_{a1}([H^+]^2 + 4K_{a2}[H^+] + K_{a1}K_{a2})}{([H^+]^2 + K_{a1}[H^+] + K_{a1}K_{a2})^2}\right)_n)$$

where $[H^+]$ is hydrogen ion concentration (mol L^{-1}, equals 10^{-pH}), $C_{i,n}$ is concentration of respectively a monoprotic or biprotic weak acid (mol L^{-1}). K_a, K_{a1} and K_{a2} are acid dissociation

constants. Since concentrations of all monoprotic and biprotic weak acids are assumed to be the same, the buffering capacity is linearly correlated with the amount of SOM.

References

French, H. M.: The Periglacial Environment, 3rd ed., John Wiley & Sons, Chichester, 2007.

Hanselmann, K. W.: Microbial energetics applied to waste repositories, Experientia, 47, 645-687, https://doi.org/, 1991.

Herndon, E., Yang, Z., and Gu, B.: Soil Organic Carbon Degradation during Incubation, Barrow, Alaska, 2012, Next Generation Ecosystem Experiments Arctic Data Collection, https://doi.org/10.5440/1168992, 2017.

Herndon, E. M., Mann, B. F., Roy Chowdhury, T., Yang, Z., Wullschleger, S. D., Graham, D., Liang, L., and Gu, B.: Pathways of anaerobic organic matter decomposition in tundra soils from Barrow, Alaska, Journal of Geophysical Research-Biogeosciences, 120, 2345-2359, https://doi.org/10.1002/2015JG003147, 2015.

Hunter, J. D.: Matplotlib: A 2D Graphics Environment, Comput. Sci. Eng., 9, 90-95, https://doi.org/10.1109/MCSE.2007.55, 2007.

Jin, Q., and Bethke, C. M.: The thermodynamics and kinetics of microbial metabolism, Am. J. Sci., 307, 643-677, https://doi.org/10.2475/04.2007.01, 2007.

Jin, Q., and Kirk, M. F.: Thermodynamic and Kinetic Response of Microbial Reactions to High CO2, Front. Microbiol., 7, 1696, https://doi.org/10.3389/fmicb.2016.01696, 2016.

Koven, C. D., Riley, W. J., Subin, Z. M., Tang, J. Y., Torn, M. S., Collins, W. D., Bonan, G. B., Lawrence, D. M., and Swenson, S. C.: The effect of vertically resolved soil biogeochemistry and alternate soil C and N models on C dynamics of CLM4, Biogeosciences, 10, 7109-7131, https://doi.org/10.5194/bg-10-7109-2013, 2013.

Liljedahl, A. K., Boike, J., Daanen, R. P., Fedorov, A. N., Frost, G. V., Grosse, G., Hinzman, L. D., Iijma, Y., Jorgenson, J. C., Matveyeva, N., Necsoiu, M., Raynolds, M. K., Romanovsky, V. E., Schulla, J., Tape, K. D., Walker, D. A., Wilson, C. J., Yabuki, H., and Zona, D.: Pan-Arctic ice-wedge degradation in warming permafrost and its influence on tundra hydrology, Nature Geosci, 9, 312-318, https://doi.org/10.1038/ngeo2674, 2016.

Oliphant, T. E.: Python for Scientific Computing, Comput. Sci. Eng., 9, 10-20, https://doi.org/10.1109/MCSE.2007.58, 2007.

Roy Chowdhury, T., Herndon, E. M., Phelps, T. J., Elias, D. A., Gu, B., Liang, L., Wullschleger, S. D., and Graham, D. E.: Stoichiometry and temperature sensitivity of methanogenesis and CO_2 production from saturated polygonal tundra in Barrow, Alaska, Global Change Biol., 21, 722-737, https://doi.org/10.1111/gcb.12762, 2015.

Sarkar, D.: Lattice: Multivariate Data Visualization with R, Springer-Verlag, New York, 2008.

Tang, G., Zheng, J., Xu, X., Yang, Z., Graham, D. E., Gu, B., Painter, S. L., and Thornton, P. E.: Biogeochemical modeling of CO_2 and CH_4 production in anoxic Arctic soil microcosms, Biogeosciences, 13, 5021-5041, https://doi.org/10.5194/bg-13-5021-2016, 2016.

Thornton, P. E., and Rosenbloom, N. A.: Ecosystem model spin-up: Estimating steady state conditions in a coupled terrestrial carbon and nitrogen cycle model, Ecol. Model., 189, 25-48, https://doi.org/10.1016/j.ecolmodel.2005.04.008, 2005.

van der Walt, S., Colbert, S. C., and Varoquaux, G.: The NumPy Array: A Structure for Efficient Numerical Computation, Comput. Sci. Eng., 13, 22-30, https://doi.org/10.1109/MCSE.2011.37, 2011.

Venables, W. N., and B.D., R.: Modern Applied Statistics with S, Springer-Verlag, New York, 498 pp., 2002.

Wickham, H.: ggplot2: Elegant Graphics for Data Analysis, Springer-Verlag, New York, 213 pp., 2009.

Yang, Z., Wullschleger, S. D., Liang, L., Graham, D. E., and Gu, B.: Effects of warming on the degradation and production of low-molecular-weight labile organic carbon in an Arctic tundra soil, Soil Biol. Biochem., 95, 202-211, https://doi.org/10.1016/j.soilbio.2015.12.022, 2016.

Zheng, J., RoyChowdhury, T., and Graham, D. E.: CO_2 and CH_4 Production and CH_4 Oxidation in Low Temperature Soil Incubations from Flat- and High-Centered Polygons, Barrow, Alaska, 2012, Next Generation Ecosystem Experiments Arctic Data Collection, https://doi.org/10.5440/1288688, 2017.

Zheng, J., and Graham, D. E.: Soil Organic Carbon Degradation in Low Temperature Soil Incubations from Flat- and High-Centered Polygons, Barrow, Alaska, 2012-2013, Next Generation Ecosystem Experiments Arctic Data Collection, https://doi.org/10.5440/1393836, 2018.
Zheng, J., RoyChowdhury, T., Yang, Z., Gu, B., Wullschleger, S. D., and Graham, D. E.: Impacts of temperature and soil characteristics on methane production and oxidation in Arctic tundra, Biogeosciences, 15, 6621-6635, https://doi.org/10.5194/bg-15-6621-2018, 2018.

Table S1 Model parameter values for reactions A1-A5 (Appendix A)

Reaction	k_{max} (d^{-1})	k_D (μM)
A1	0.83	
A2	0.5	12
A3	0.8	11
A4	0.3	23
A5	0.5	4.7

Table S2 Initial conditions used for model simulations

Treatment ID	SOC (mol)	TOTW (mL)	TOAC (mM)	pH	Fe(II) (mM)	f_{doc}	Me_biomass (mol C)	Fe_biomass (mol C)
LCP-C1-O[1]	0.05	13.6	6.37	5.0	0.79	0.02	8e-5	2e-5
LCP-C1-M	0.11	5.9	2.78	4.8	22.23	0.01	4e-6	1e-5
LCP-C2-M	0.15	5.2	0.47	5.9	2.7	0.01	4e-6	5e-7
LCP-C2-P	0.02	2.8	4.05	7.1	5.0	0.02	5e-8	2e-7
LCP-R-O	0.10	11.8	0.06	5.2	1.62	0.02	5e-6	1e-5
LCP-R-M	0.11	6.4	2.67	4.5	22.97	0.01	2e-5	2e-5
LCP-T-O	0.07	10.7	1.03	5.2	15.67	0.02	1e-5	5e-6
LCP-T-M	0.06	6.6	1.84	5.0	7.18	0.01	8e-6	1e-5
FCP-C-T	0.02	7.1	2.15	4.9	20.24	0.02	1e-6	1e-5
FCP-C-P	0.08	8.0	10.76	5.0	17.45	0.02	2e-7	2e-6
HCP-C1-M	0.14	4.8	12.58	5.92	113.98	0.01	-	1e-9
HCP-C2-P	0.14	8.2	8.57	7.06	17.92	0.02	-	1e-9
HCP-T-O	0.26	4.9	39.87	5.1	25.62	0.01	5e-7	1e-6
HCP-T-M	0.14	5.8	2.84	5.3	20.92	0.01	2e-6	1e-8

[1] Notations of treatment (soil microtopographic feature × soil layer combination) are abbreviated as follows: LCP, Low-centered polygon; FCP, Flat-centered polygon; HCP, High-centered polygon; C, Center; T, Trough; R, Rim; O, Organic; M, Mineral; P, Permafrost. For example, LCP-C1-O means Low-Centered Polygon-Center (the first soil core)- Organic layer.

Table S3 Model fitted fermentation rate for each soil microcosm (at 4 °C)

Treatment ID	f_{fer} (day^{-1})	R^2
LCP-C1-O	5.58E-03	0.77
LCP-R-O	1.39E-03	0.72
LCP-T-O	5.58E-03	0.82
HCP-T-O	7.97E-05	0.50
LCP-C1-M	1.39E-04	0.72
LCP-R-M	1.39E-04	0.79
LCP-T-M	2.79E-05	0.86
FCP-C-T	1.39E-05	0.65
LCP-C2-M	5.58E-04	0.73
HCP-C-M	5.58E-05	0.66
HCP-T-M	6.97E-06	0.82
FCP-C-P	1.61E-10	0.50
LCP-C2-P	8.07E-11	0.44
HCP-C2-P	3.23E-14	0.32

Table S4 Descriptive statistics and correlation matrix for soil attributes and labile carbon pool

	1	2	3	4	5	6	7	8a/8b
1. SOC								
2. WEOC	0.80[a]							
3. TOAC	0.62	0.69[a]						
4. Moisture	0.69[a]	0.82[a]	0.78[a]					
5. pH	-0.30	-0.15	-0.14	-0.11				
6. C/N ratio	0.07	0.06	0.17	0.05	-0.64 [b]			
7. Fe(II)	0.06	0.09	0.15	0.04	-0.35	-0.03		
8a. Max_8_CO_2[c]	0.75[a]	0.72[a]	0.55[b]	0.81[a]	-0.15	-0.03	-0.28	
8b. Max_2_CO_2	0.66[a]	0.73[a]	0.77[a]	0.90[a]	-0.12	0.11	-0.24	
9a. Max_8_CH_4	0.54[b]	0.63[b]	0.67[a]	0.85[a]	-0.13	0.19	-0.29	0.90[a]
9b. Max_2_CH_4	0.47	0.61[b]	0.75[a]	0.84[a]	-0.09	0.22	-0.23	0.96[a]

Notes: [a] correlation is significant at the 0.01 level (two-tailed); [b] correlation is significant at the 0.05 level (two-tailed); [c] Maximal production of CO_2 and CH_4 (gas production calculated as per gram dry soil) at +8 and -2 °C were estimated after 60 days of incubation.

Table S5 ANOVA for effect of temperature and soil depth on initial production rate of CO_2 and CH_4

		F	*p*
CO_2	Temperature	3.83	0.02
	Soil depth	25.93	<0.001
	Interaction	3.90	0.005
CH_4	Temperature	3.26	0.04
	Soil depth	7.70	<0.001
	Interaction	2.29	0.07

5

Table S6 Soil depth effect on the estimated Q_{10} values of CO_2 and CH_4 production (*t*-test with unequal variances)

		t	*p*
CO_2	Organic vs. Mineral	2.36	0.85
	Organic vs. Permafrost	3.18	<0.01
	Mineral vs. Permafrost	2.31	<0.01
CH_4	Organic vs. Mineral	4.30	0.13
	Organic vs. Permafrost	4.30	0.09
	Mineral vs. Permafrost	2.78	0.12

5

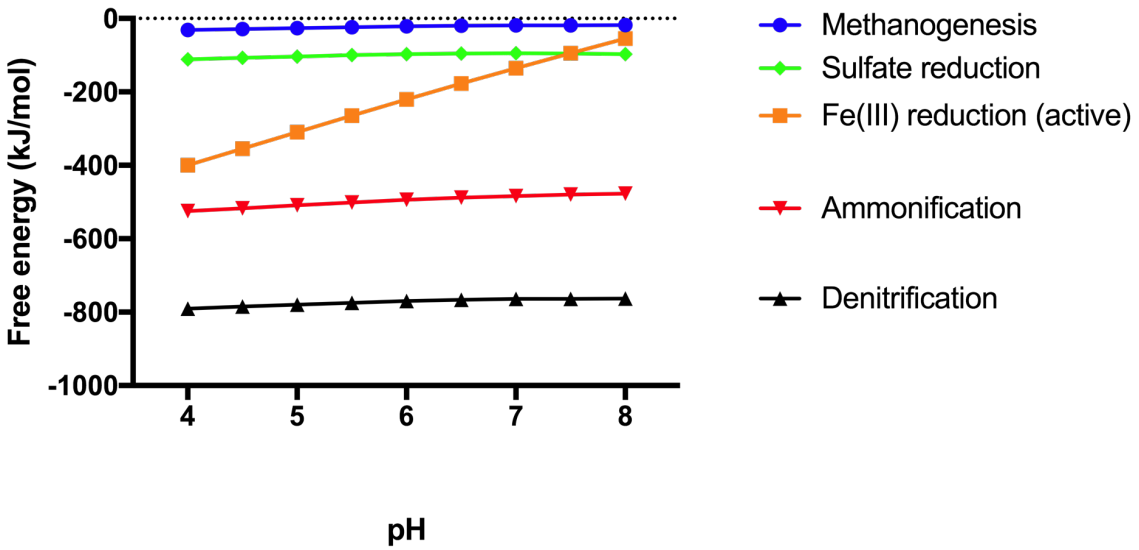

Figure S1 The Gibbs free energy of anaerobic microbial processes increases with pH. Values were calculated from standard free energies of reaction for acetate oxidation coupled to the indicated reduction processes (Hanselmann, 1991). Substrate and product concentrations were estimated from BEO polygon soil samples assuming 298 K temperature, 200 µM total dissolved CO_2 species, 1 mM $Fe(OH)_3$ equiv., 14 mM Fe(II), 374 µM acetate, 5.7 µM dissolved CH_4, 160 nM NO_3^-, 28 µM NH_4^+, and 75 µM SO_4^{2-}.

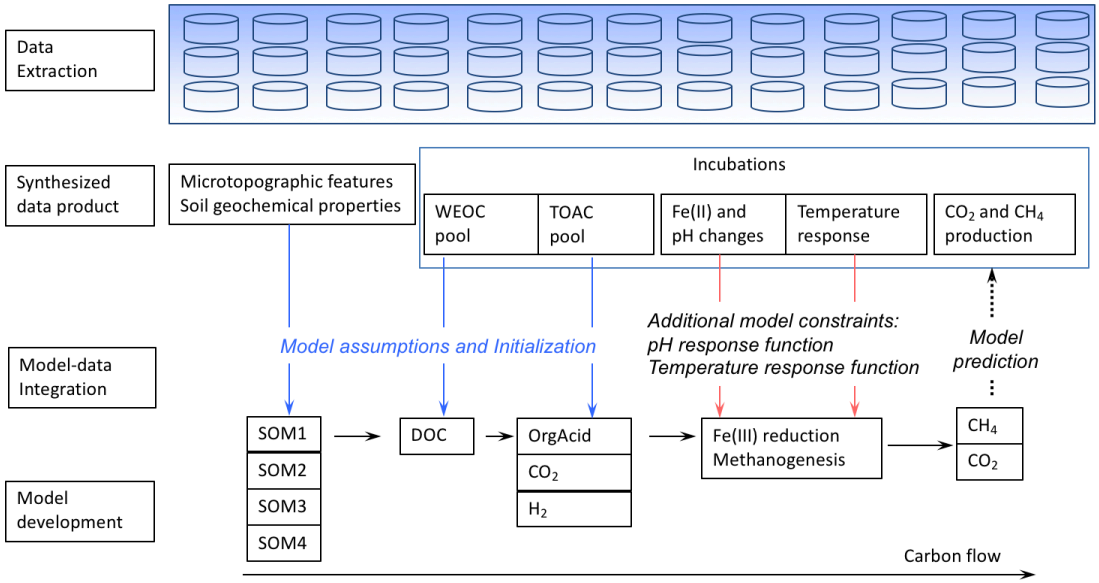

Figure S2 Flow chart of model initialization and validation with synthesized data product. Homogenized core sections, shown as cylinders, were incubated to measure CH_4 and CO_2 production rates reported previously. The data product synthesized here was used to parameterize and initialize the new model, and gas production rates were used to validate model predictions.

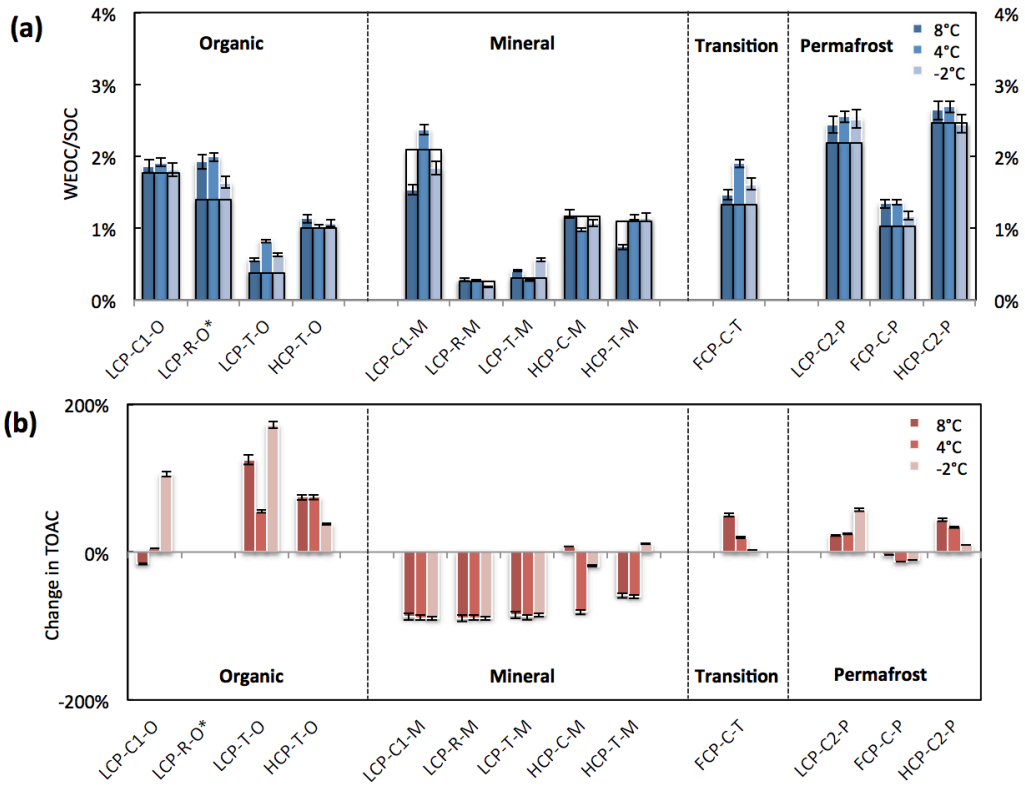

Figure S3. Changes in (a) WEOC/SOC (quotient of water extractable organic carbon to total soil organic carbon) and (b) TOAC (calculated as ($TOAC_{after}$ - $TOAC_{before}$)/$TOAC_{before}$) after anaerobic incubations at -2, 4 and 8 °C. Bars framed with black lines in panel (a) represent the TOAC/WEOC levels before incubation, and blue bars represent levels after the incubation at corresponding temperatures. Error bars represent standard deviations among triplicate incubations.

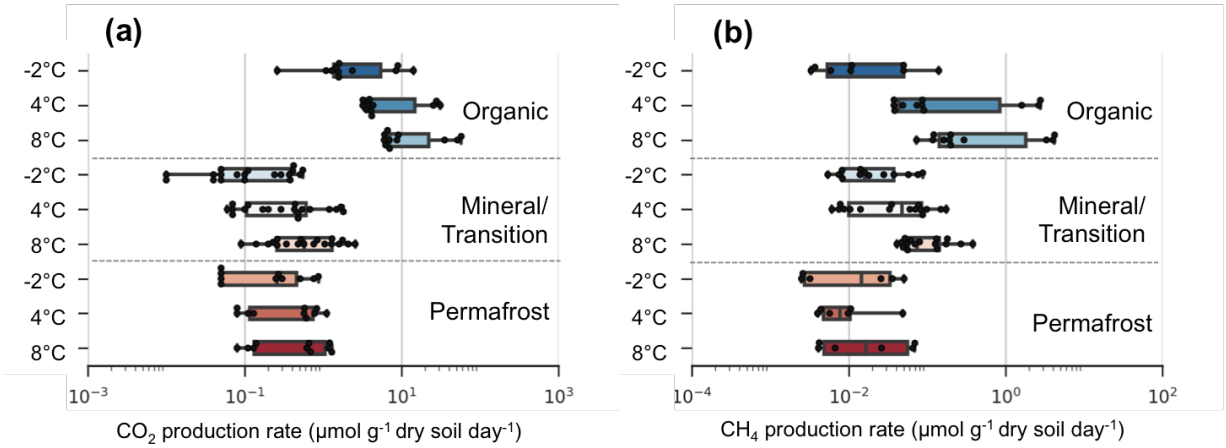

Figure S4. Box plots show temperature effects on (a) CO_2 and (b) CH_4 production rates grouped by soil layer. Samples in the transition zone from FCP were pooled with other mineral soils. The two ends of the box represent the 25th and 75th percentile and the lines extending from the box are the 10th and 90th percentile. Please note rates are plotted on log scales.

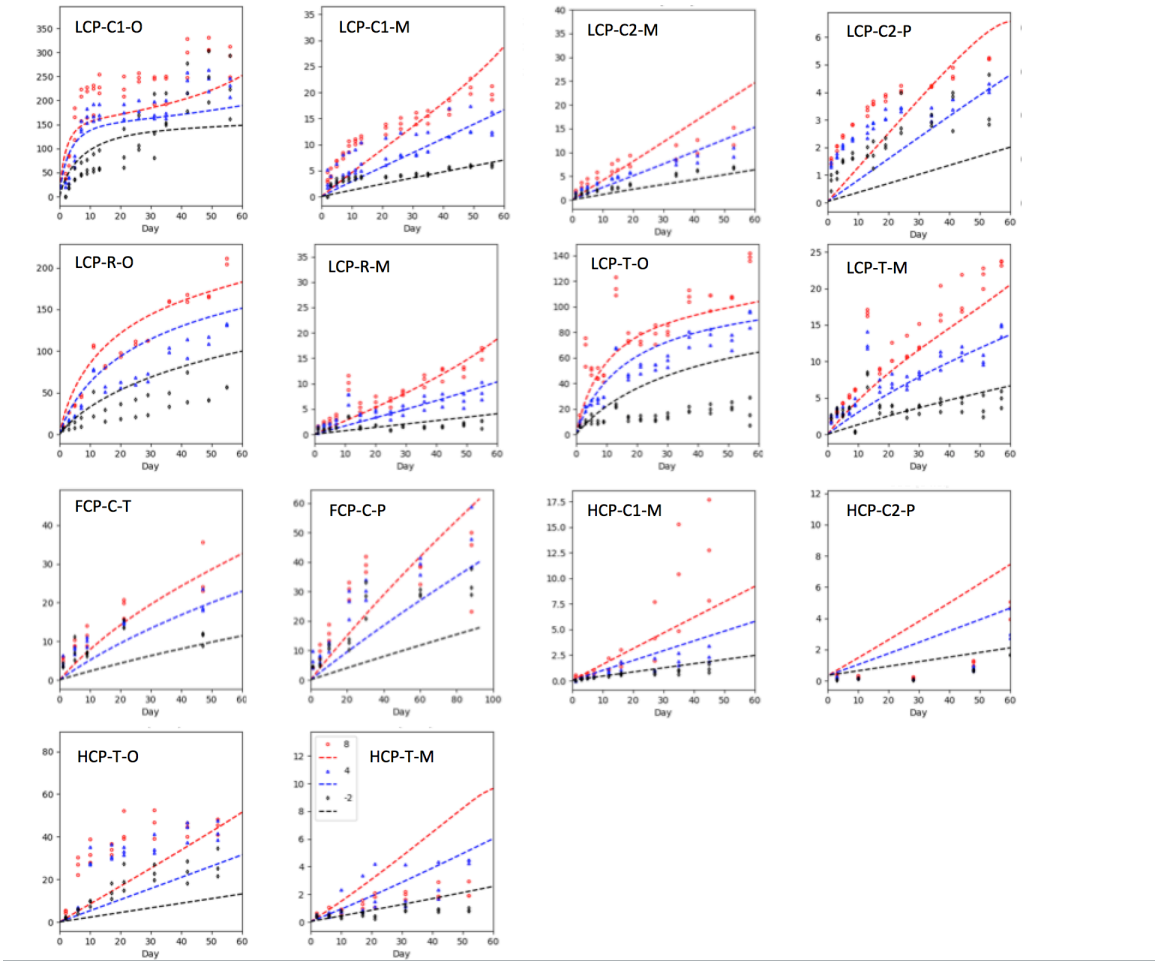

Figure S5 Comparison of observed and modeled CO_2 production from organic, mineral (transitional) and permafrost layers of different microtopographic features of LCP, FCP and HCP.

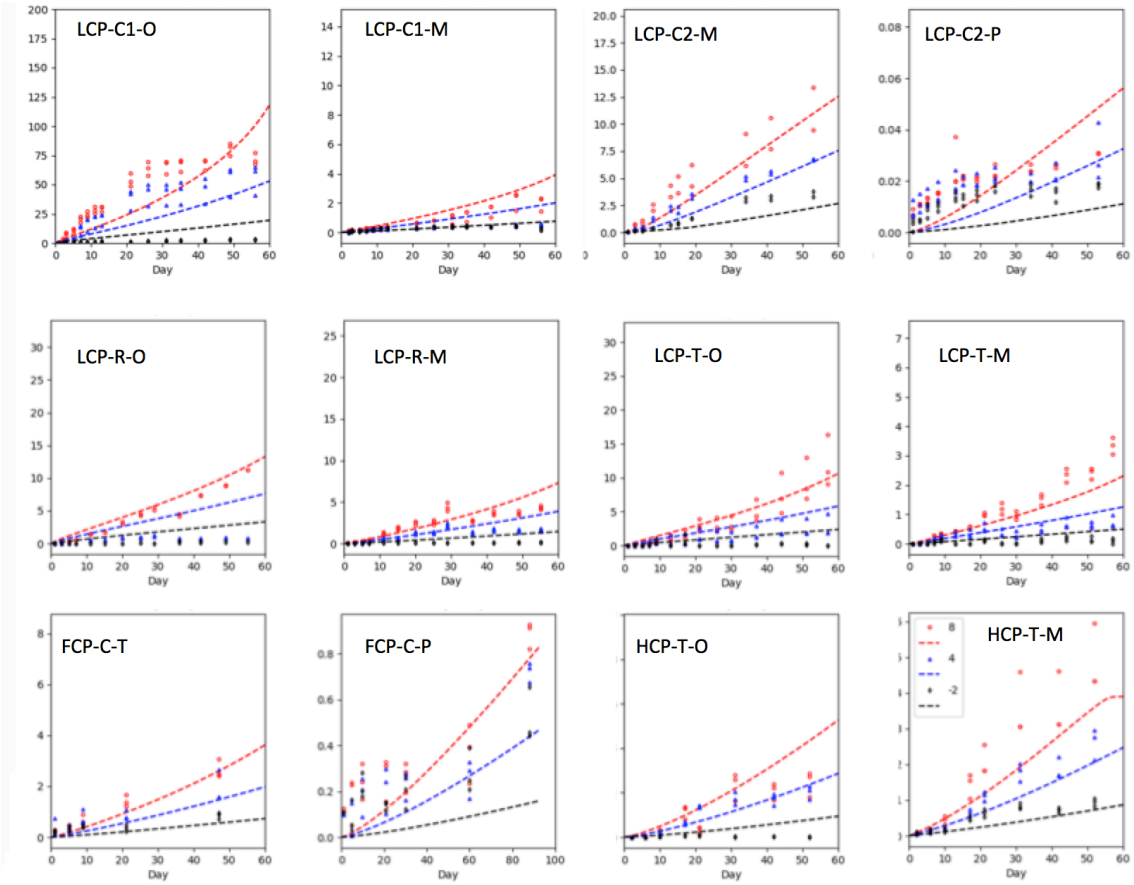

Figure S6 Comparison of observed and modeled CH_4 production from organic, mineral (transitional) and permafrost layers of different microtopographic features of LCP, FCP and HCP.

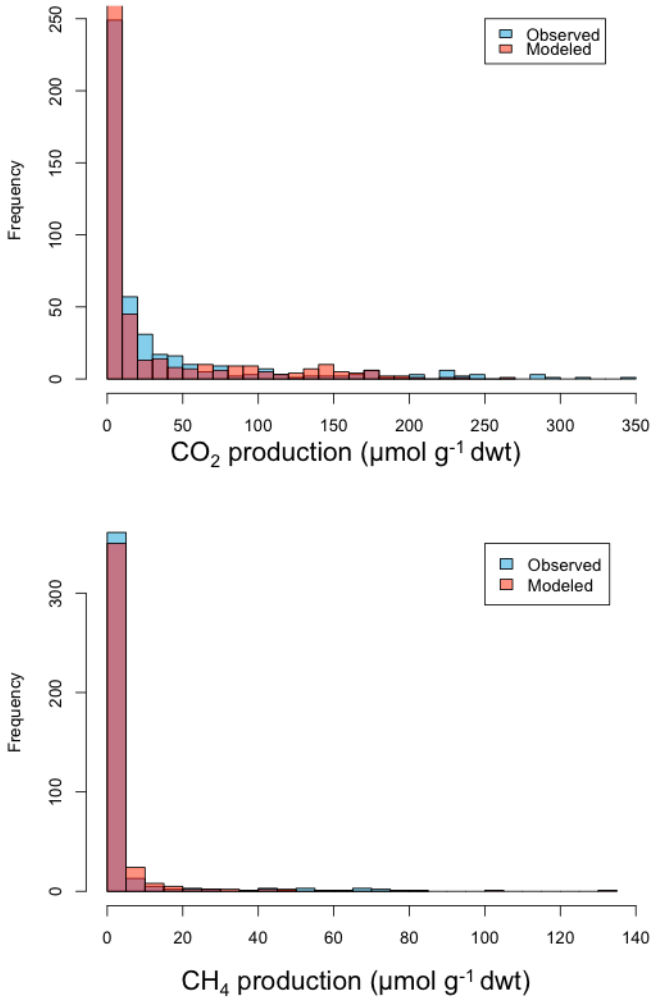

Figure S7 Comparison of data distribution between modeled and observed values for both CO_2 (upper) and CH_4 (lower) production.

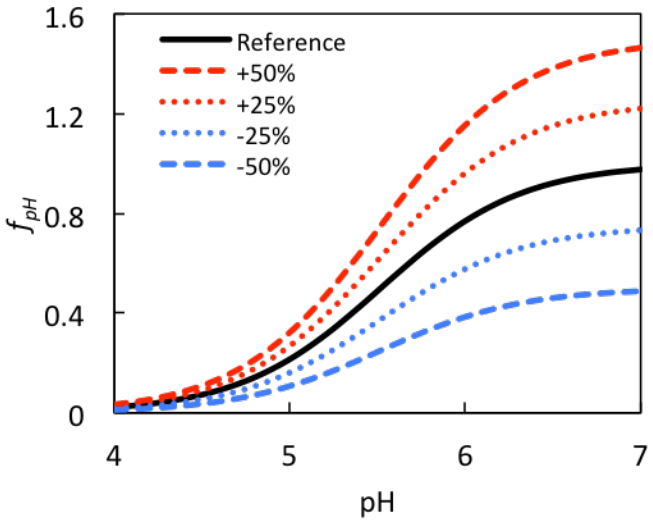

Figure S8. pH response functions used in sensitivity analysis. Perturbations of ±25% and ±50% perturbations to the final value of f_{pH}.

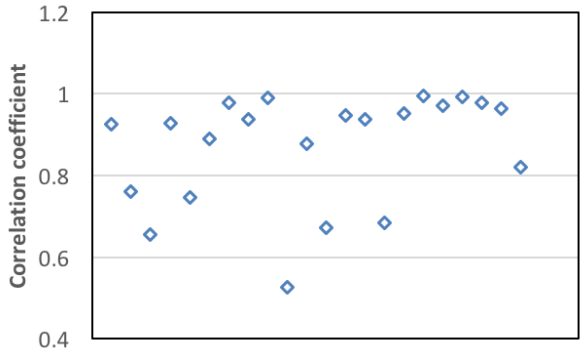

Figure S9 Correlations between Fe(II) concentration increase and pH increase during anaerobic incubations of LCP and FCP samples.

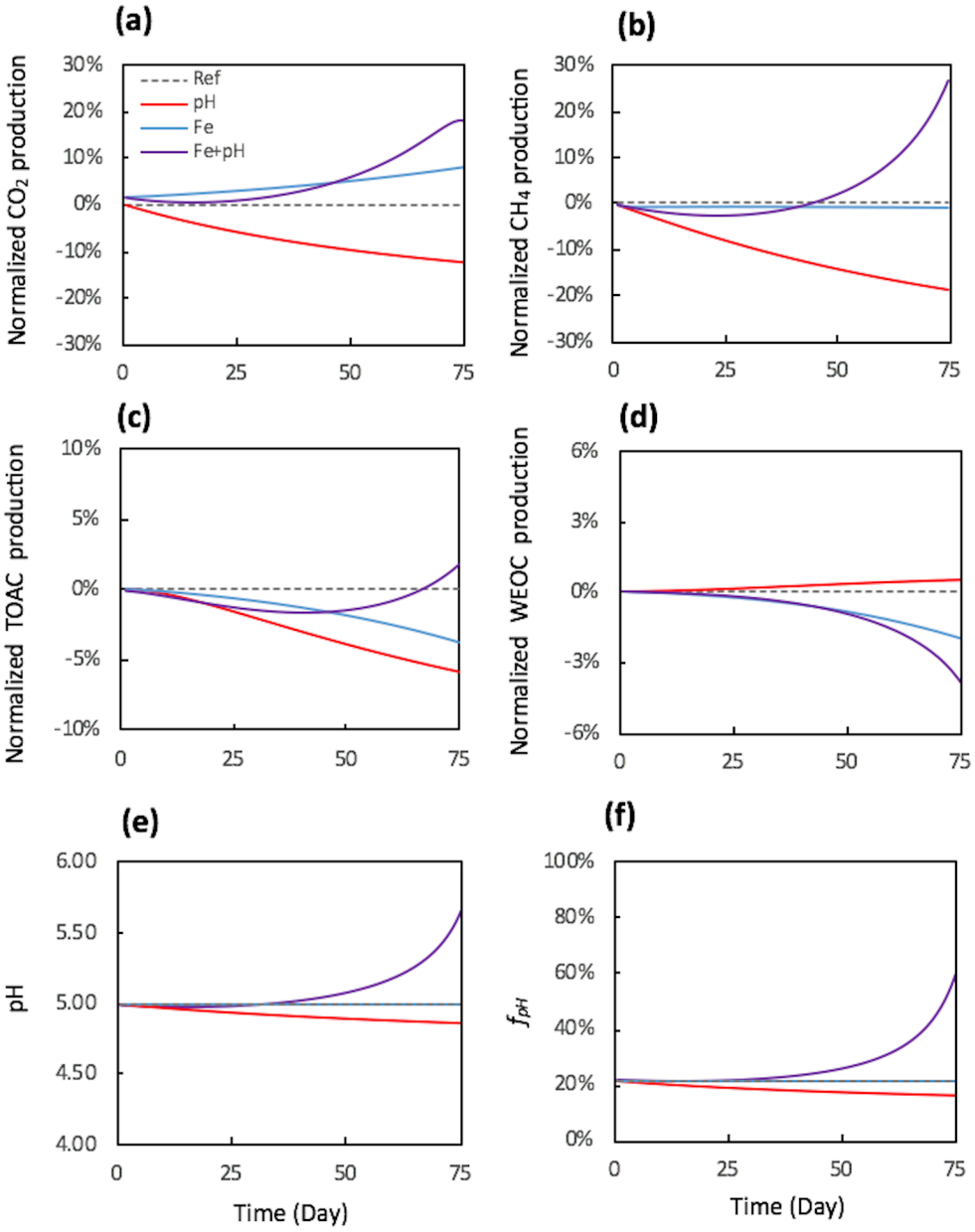

Figure S10. Model sensitivity analysis with and without Fe reduction or dynamic pH calculation model components. The baseline reference run (Ref) was based on a model structure without Fe reduction and dynamic pH calculation using soils with 30% SOC (water content=2 g g^{-1} dwt, and pH=5). Perturbation simulations were based on model structures with Fe reduction (Fe), dynamic pH calculation (pH), and both Fe reduction and dynamic pH calculation (Fe+pH). (a, b) Normalized changes in simulated CO_2 and CH_4 production, (c, d) Normalized changes in the accumulation of TOAC and WEOC, (e, f) Corresponding pH and f_{pH} dynamics. Reference simulations were based on soils with 30% SOC (water content=2 g g^{-1} dwt, and pH=5). Normalized changes in model output were calculated as the ratio of changes caused by perturbation simulations (differences between perturbation and reference runs) to reference simulation output.